Eigenvalue Statistical Components-Based PU-Learning for PolSAR Built-Up Areas Extraction and Cross-Domain Analysis

Rong Gui, *Graduate Student Member, IEEE*, Xin Xu, Lei Wang, *Member, IEEE*, Rui Yang, *Graduate Student Member, IEEE*, and Fangling Pu, *Member, IEEE*

***Abstract*—Polarimetric synthetic aperture radar (PolSAR) provides important support for the built-up areas (BA) information analysis, due to the ability of weather-independent imaging and sensitivity to targets scattering and geometric characteristics. However, PolSAR BA with large orientation angles is usually misdetected as vegetation, and labeled BA samples with special orientations are difficult to obtain. Furthermore, the labeled BA samples and trained models can hardly work well in the cross-domain PolSAR imagery BA analysis. This article presents a PolSAR BA extraction method based on eigenvalue statistical components (ESC) and PU-Learning (PUL), and it helps to realize cross-domain BA extraction by combining subspace alignment (SA). First, the roll invariance of coherency-matrix eigenvalues and building orientation effects are analyzed. Then, by adopting the eigenvalue-Wishart unsupervised classification, regional statistical information and rotation-invariant property are comprehensively utilized in ESC. Finally, the BA can be extracted by combining a PUL classifier with only positive samples at the same distinguishable orientation. Combined with SA, the novel ESC-PUL-SA domain adaptation facilitates a robust unsupervised cross-domain PolSAR BA analysis, reducing the differences caused by sensors and imaging scenes. The ESC-PUL BA extraction on seven PolSAR imageries showed that the accuracies reach 92%–98% with only a few positive samples (less than 0.65%). The ESC-PUL-SA performance was further validated by 14 unsupervised cross-domain BA analysis units among 10 datasets, including Radarsat-2, Gaofen-3, AirSAR, and UAVSAR images. With randomly selected positive samples from the source domain, the proposed ESC-PUL-SA achieved accuracies of all cross-domain BA extraction range from 89.64% to 95.53%.**

***Index Terms*—Built-up areas (BA), eigenvalue statistical, polarimetric synthetic aperture radar (PolSAR), PU-learning (PUL), roll invariance, unsupervised domain adaptation (DA).**

I. Introduction

ACCURATE and timely built-up areas (BA) information analysis provide valuable supports for many applications, such as the evaluation of ecological environment [1], urban expansion and planning [2], [3], fast response to natural disasters [4], [5], etc. With the ability of weather-independent imaging and sensitivity to targets' scattering and geometric characteristics, polarimetric synthetic aperture radar (PolSAR) has demonstrated its potential in BA extraction [6]–[8]. However, due to the high complexity of BA structure composition and the orientation angle problems [8], [9], extracting BA accurately from PolSAR is still a challenging task [6], [10]. For most supervised PolSAR BA extraction methods, labeling enough positive BA samples with special orientations is difficult and time consuming. Also, the negative labels for BA tasks are usually unavailable, since the background categories are always uncertain [11]. Furthermore, the labeled BA samples and trained models can hardly work well in cross-domain BA analysis tasks [12]. These problems impede the further development of accurate and timely BA extraction and change monitoring applications from PolSAR data.

Extensive methods based on scattering model decompositions [13] have been studied for the PolSAR BA analysis, but the misclassifications of BA with obliquely oriented buildings [7], [15] as vegetation areas are still a regular occurrence in practical applications. The well-known orientation angle compensation developed on scattering model decomposition can improve the misclassification to some extent, but this process is not always effective when the rotation angle exceeds a certain limit [7], [9]. In addition, some special polarization decomposition methods are proposed to improve the overestimation of volume scattering components toward BA, typically, e.g., general polarimetric model-based decomposition [16], and eigenvalue-related decomposition model for BA extraction [9], [14]. Otherwise, some approaches utilize a separate class for identifying rotated BA [17], [18], and merge them with the nonrotated BA as a postclassification step. However, these methods increase the difficulty of sample labeling and postprocessing. Recently, polarimetric features with roll invariance and complex-valued information have attracted much attention for SAR image classification [19], [20] and man-made targets extraction [9], [14], [21]–[23]. The coherency-matrix eigenvalues and some derivative parameters have been applied to identify BA at pixel level, due to the roll invariance, straightforward, and easily calculated.

On the other hand, increasing amounts of PolSAR images from different sensors and different scenes are available, and

Manuscript received January 20, 2020; revised April 1, 2020 and May 14, 2020; accepted June 1, 2020. Date of publication June 9, 2020; date of current version June 22, 2020. This work was supported in part by the National Key Research and Development Program of China under Grant 2018YFB2100503 and in part by the Thirteen-Five Civil Aerospace Planning Project-Integration of Communication, Navigation and Remote Sensing Comprehensive Application Technology. *(Corresponding author: Xin Xu.)*

The authors are with the School of Electronic Information, Wuhan University, Wuhan 430072, China (e-mail: ronggui2013@whu.edu.cn; xinxu@whu.edu.cn; wanglei2016@whu.edu.cn; ruiyang@whu.edu.cn; flpu@whu.edu.cn).

Digital Object Identifier 10.1109/JSTARS.2020.3000743

recent successes in machine learning or deep learning [7] always rely on the availability of very large labeled samples. But obtaining sufficient and reliable labeled information is always an important bottleneck for PolSAR interpretation studies [12], [24]. If the abovementioned orientation problems cannot be well solved, then they usually require lots of labeled BA samples with various orientations, which are extremely unfavorable for the fast and accurate acquiring BA information from PolSAR imagery. Furthermore, BA extraction problem can be considered as extracting targets from various kinds of backgrounds, i.e., water, forest, and grassland. Labeling these negative samples in PolSAR imagery is also difficult, expensive, and time consuming, and the background categories are usually uncertain. Therefore, it is especially necessary to develop methods for PolSAR BA interpretation under weak-supervised or unsupervised conditions, due to the unavailability of enough labeled data. Methods that are beneficial to alleviate the sample labeling problems, such as active learning [25], weakly supervised learning [26], and zero/few-shot learning [24], have been gradually studied in SAR BA interpretation.

Recent years, how to effectively transfer the accurate supervised information of existing data to abundant newly acquired data with similar scenarios is emerging as research hotspot and difficulty in SAR interpretation [27], [28]. There are similar problems in long-term monitoring about BA expansion and changing applications. It can hardly apply rare BA samples from source domain to another newly acquired target data directly, even if the scenes of these domains are similar. These domain shift problems [29] are generally caused by differences in sensors, acquisition conditions, imaging scenes, and even wavebands. Furthermore, as the particularity of SAR imaging, the classical or optical remote sensing (RS) cross-domain methods always cannot be applied to SAR cross-domain BA interpretation directly. These problems provide higher requirements for the PolSAR image BA analysis. That is, PolSAR BA interpretation systems should be robust for SAR acquisition conditions, temporal shifts and, ideally, be adaptive to sensor differences, and the algorithms should own the ability of cross-domain interpretation, rather than simple homologous supervised classification.

In order to extract BA from PolSAR imagery with only a few positive samples, and to further apply labeled positive samples into the cross-domain data BA analysis, this article focuses on addressing the abovementioned problems by eigenvalue statistical components (ESC) and learning from positive and unlabeled data (PU-Learning, PUL) [30]–[32]. First, the roll invariance of coherency-matrix eigenvalues and the building orientation effects are analyzed. Then, by adopting the eigenvalue-Wishart unsupervised classification, regional statistical information and rotation invariant property are comprehensively utilized by ESC at a patch level. Third, the BA can be extracted by combining a PUL classifier with only positive samples at a same distinguishable orientation. Combining with the unsupervised domain adaptation ability of subspace alignment (SA) [33], [34], the proposed ESC-based PUL (ESC-PUL) has further proved its ability for unsupervised cross-domain PolSAR BA analysis (ESC-PUL-SA).

In the proposed frameworks, the polarimetric eigenvalues are employed to overcome the BA misdetection caused by large orientation angels. Considering that BA possesses regional characteristics and contains various complex man-made targets, we use region-based eigenvalue Wishart statistics to express the polarimetric and regional characteristics of BA. Then, to reduce the dependence on abundant sample labeling, the PUL classifier is used to extract BA, only through a small number of obvious positive samples. Moreover, the ESC-PUL-SA facilitates robust unsupervised cross-domain PolSAR BA extraction and expansion analysis, reducing the differences caused by sensors and imaging scenes.

This article is a substantial extension of the conference version published in [35]. Compared with the preliminary version, this article has made following major extensions.

1) Providing more thorough literature backgrounds, including roll-invariance features and building orientation effect, PUL, and cross-domain RS BA analysis.
2) Several state-of-the-art methods are compared, to show the advantages of proposed ESC-PUL.
3) Extending and evaluating the ESC-PUL method for unsupervised cross-domain BA analysis where labeled samples are not present in target domains, with only positive samples from source domain available.
4) Evaluating the effect of cross-domain BA analysis among Radarsat-2, Gaofen-3, AIRSAR, and UAVSAR PolSAR data.
5) Expanding the experiment section by analyzing the large scenes BA expansion of Wuhan Optical Valley region from Radarsat-2 and Gaofen-3 PolSAR data.

The remainder of this article is organized as follows. Section II provides an overview of background and related works. In Section III, the proposed ESC-PUL framework for BA extraction, as well as the ESC-PUL-SA for unsupervised cross-domain PolSAR BA analysis, is presented. Section IV describes the datasets, experimental setting, results, and discussion. Conclusions and future directions are drawn in Section V.

II. Background and Related Works

Brief study overviews of building orientation angle (BOA) and polarization orientation angle (POA) are provided here, followed by essential introduction to roll-invariant features, PUL, and cross-domain RS BA analysis.

A. Roll-Invariant Features and Building Orientations

BA shows large intraclass differences in PolSAR imagery, due to the various orientation differences and complex structures. When the angle α (BOA) between SAR azimuth direction and the direction of building block walls is large (the obliquely oriented buildings), as shown in Fig. 1(a), the double-bounce scattering of BA is weak [7]–[9], and the volume scattering is often overestimated. Traditional model decomposition-based methods tend to misdetect these oriented BA as vegetation [9], [13], [15].

The POA θ, as shown in Fig. 1(b), is defined by the angle between major axis of polarization ellipse and horizontal axis [36],

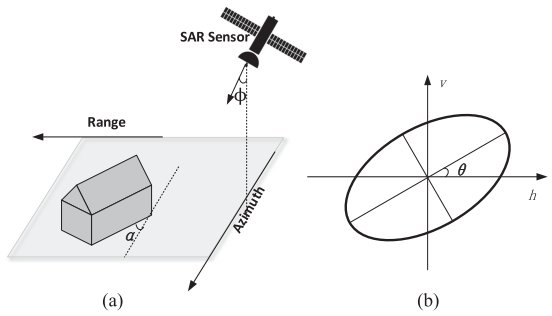

Fig. 1. Illustration of POA and BOA. (a) BOA. (b) POA.

[37]. In recent years, POA gets a lot of attention in the PolSAR imagery BA analysis. It is been derived that from the scattering model of BA in horizontal ground [15], [36]; the POA shift θ in BA can be given as follows:

$$\tan\theta = \frac{-\tan\alpha}{\cos\phi} \tag{1}$$

where α is BOA, and ϕ is radar incidence angle [as illustrated in Fig. 1(a)]. From the abovementioned analysis, it can be seen that the tangents of BOA and POA have a linear relationship in horizontal ground, in the case of a certain incident angle ϕ. In the following, the polarimetric features with roll invariance are employed to overcome the misdetection of BA with large BOA.

Polarimetric coherency matrix $\mathbf{T}$ is a 3×3 Hermitian and positive semidefinite matrix having complex Wishart distribution [37]. So it can be diagonalized as following:

$$\mathbf{T} = \mathbf{U}\mathbf{\Lambda}\mathbf{U}^{-1}. \tag{2}$$

$\mathbf{\Lambda}$ is a real diagonal matrix containing the eigenvalues of $\mathbf{T}$

$$\mathbf{\Lambda} = \begin{bmatrix} \lambda_1 & 0 & 0 \\ 0 & \lambda_2 & 0 \\ 0 & 0 & \lambda_3 \end{bmatrix} \tag{3}$$

where $\infty > \lambda_1 \geq \lambda_2 \geq \lambda_3 > 0$. The 3×3 complex unitary matrix $\mathbf{U}$ contains the eigenvectors of $\mathbf{T}$. The eigenvalues of $\mathbf{T}$ are roll-invariant parameters; furthermore, some eigenvalues derivative parameters are also roll-invariant, e.g., the radar vegetation index (RVI) and entropy (H), and mean magnitude of the mechanism ($\bar{\lambda}$) [37]. The polarimetric feature parameters with roll-invariant characteristics are not affected by POA shifts and regardless of target orientation diversity effect, so they are suitable for classification and target recognition in lands with small terrain slopes or most urban areas [13], [36].

B. PU-Learning

The model of learning from positive and unlabeled data has emerged as a method that significantly reduces manual labeling and does not require a complete set of negative samples [11], [38]. In PUL, the training data are composed of a small positive samples set and a larger unlabeled samples set, which can be positive or negative [39]. PUL assumes that a large amount of unlabeled data are available, and aims to fully exploit the unlabeled data together with the limited positive data to learn more precise predictive models. PUL is generally composed of two steps to classify the unlabeled samples, the first step is to identify negative samples from an unlabeled set, and the second is using obtained negative and positive samples to train a binary classifier [11], [39].

PUL was first applied to solve binary text classification problems for which no negative training data exist [11]. Recent years, PUL is proved to be conceivable in various applications such as land-cover classification [40], where positive samples (e.g., BA) can be easily obtained, but negative samples are too diverse to be labeled. Outlier detection in unlabeled data based on inlier data can also be regarded as PUL classification [41]. Considering that PUL can alleviate the difficulty of sample labeling and the reliable learning strategy of negative samples, this article applies PUL for BA extraction and cross-domain BA analysis.

By using a small number of common-oriented BA samples, the roll invariant characteristics was combined with PUL, it can overcome the orientation characteristics to extract the BA. This combination does not need the labeled negative samples, and the requirements for positive samples are further reduced. Furthermore, for a cross-domain BA analysis, the PUL and SA are used to learn the positive samples and negative samples in the target domain, so as to realize the unsupervised cross-domain BA analysis by a small number of positive samples from source domain.

C. Cross-Domain RS BA Analysis

Increasing amounts of PolSAR images from different sensors and different scenes are available, which can provide sufficient data source for urban expansion and change the information analysis. However, the valuable labeled samples and trained models are still hard to work well in cross-domain data interpretation. Recent years, domain adaptation (DA) shows attractive potential in RS fields, since it can transfer knowledge in existing images to new yet related images [29]. To reduce the domain shifts between source and target domains, classifier-level DA, invariant feature selection DA, and adapting feature distribution representation methods were widely studied. Among them, the adapting feature distribution representation strategy has attracted more and more attention in cross-domain RS fields [28], [29], due to the ability for unsupervised DA and flexibility.

Compared with recent rapid development of DAs in optical RS field, few studies have been conducted on PolSAR cross DA [42]. Besides, to alleviate the lack of labeled sample, knowledge from optical data [2], [6], simulated data [43], etc., has begun to be used in SAR target interpretation. Studies about BA expansion and change information from cross-domain SAR data are even fewer. The main difficulties lie in the following two aspects, the domain shifts between source and target domains, and the intraclass differences caused by building orientations, since the labeled BA samples with all orientations are not always available. Especially in the case of only a small number of positive samples available from source domain, the cross-domain BA analysis method should own the ability of overcoming influence of building orientations and learning negative samples at the same

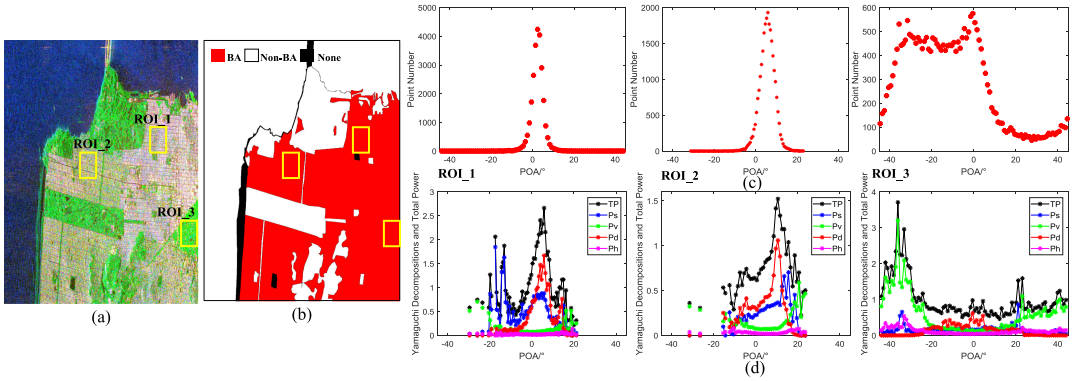

Fig. 2. Illustrations of intraclass difference problem caused by building orientations. (a) Radarsat-2 San Francisco data with color composed by Yamaguchi basis. (b) Ground truth of (a). (c) POA distribution in ROIs. (d) Relationships between Yamaguchi four components and POA distributions in ROIs.

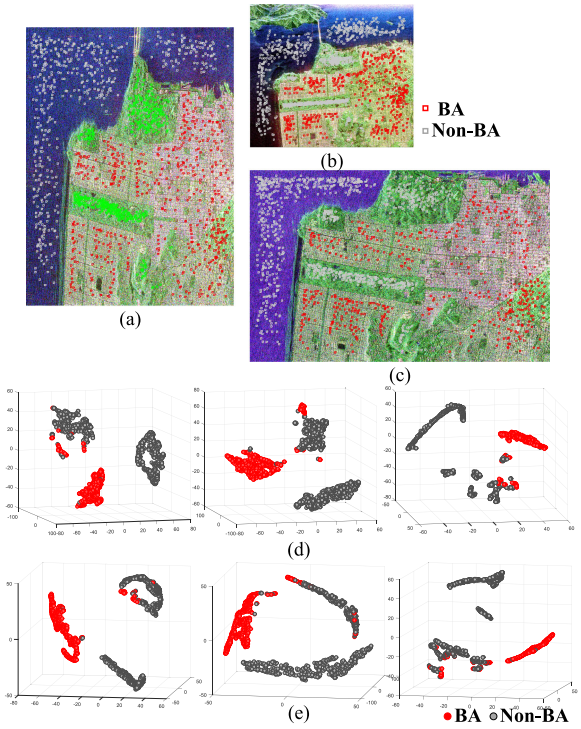

Fig. 3. Examples of domain shifts between cross-domain PolSAR data. (a) Radarsat-2 San Francisco data and samples. (b) AIRSAR San Francisco data and samples. (c) Gaofen-3 San Francisco data and samples. (d) Filtered C3 features of samples in (a)–(c) with a t-SNE view. (e) Filtered Yamaguchi decompositions features of samples in (a)–(c) with a t-SNE view.

time. Fig. 2 illustrates the intraclass difference problem caused by building orientations. The POA distributions in Fig. 2(c) can reflect the BOA differences, and the model-decomposition features are affected by the BOA, the feature of BA in ROI-3 is similar to that of forests. By using t-SNE [44] visualization, Fig. 3 shows the domain shifts between cross-domain PolSAR data.

III. Proposed Method

The proposed ESC-PUL BA extraction and ESC-PUL-SA cross-domain BA analysis are organized by three main parts,

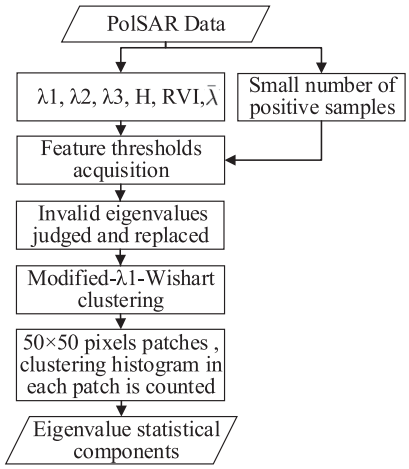

Fig. 4. ESC extraction process.

including ESC representation, ESC-based PUL for PolSAR BA extraction, and ESC-SA for cross-domain PolSAR BA analysis. In BA extraction framework, a small number of positive samples with same obvious orientation are randomly selected, negative samples and BA samples with special orientations are not required. In cross-domain BA analysis framework, there are only few positive samples from source domain available, and target domain does not contain any labeled information.

A. Eigenvalue Statistical Components

The applied ESC are obtained by the workflow in Fig. 4. The roll-invariant eigenvalues and derivative parameters are first extracted, some invalid eigenvalues are judged and replaced. Then, considering the regional characteristics of BA, modified eigenvalue-Wishart unsupervised classification is adopted at image patch level, thus, regional statistical information and roll-invariant properties are comprehensively utilized.

In detail, λ_1, λ_2, λ_3, RVI, H, $\bar{\lambda}$ are first extracted, and some invalid λ_1 values are judged and replaced by the relationship between λ_1, λ_2, λ_3 [37]. Then, the eigenvalues with high RVI, low H, or low $\bar{\lambda}$ values should also be replaced, since the regions with these properties do not meet the BA characteristics, and

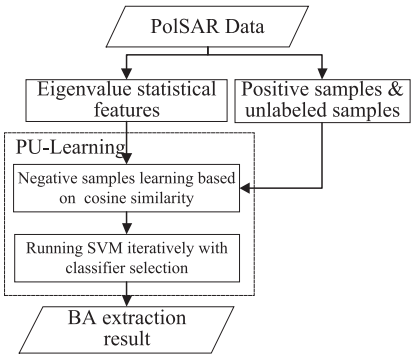

Fig. 5. Proposed workflow of PolSAR BA extraction.

there are inevitable randomness and noises in these regions [37]. The corresponding thresholds judged these regions can be determined by labeled positive samples.

As λ_1 is eigenvalue of the dominant scattering, and λ_2 and λ_3 are vulnerable to noise, the modified λ_1 obtained by aforementioned two rounds of replacements is applied. Inspired by the fact that unsupervised classification based on scattering mechanisms and Wishart classifier has been widely applied in PolSAR interpretation [13], here the Wishart clustering is employed on the modified λ_1 feature. Also, the clustering information is statistically analyzed at image patches level to form the statistical features. This Wishart statistical has been proved to be widely applicable to PolSAR data [13], [37]. The Wishart distance D_{ij} between two clusters V_i and V_j is calculated as follows. The cluster V_i obtained by initial clustering the modified-λ_1 features

$$D_{ij} = \frac{1}{2}\left\{\ln(|V_i|) + \ln(|V_j|) + \mathrm{Tr}(V_i^{-1}V_j + V_j^{-1}V_i)\right\}. \quad (4)$$

The PolSAR data applied in this article are mainly with 8-m resolution; thus, the patch size of 50 × 50 pixels can hold composition of different BA and capture sufficient context information. The dimension of the applied statistical features is 32 (adjustable). The ESC features aim to overcome the orientation influences shown Fig. 2. In ESC, the roll-invariant features help to overcome the BA orientation effects, and the Wishart statistical components in region level further integrate the structure and texture properties in BAs.

B. ESC-Based PUL for PolSAR BA Extraction

The proposed BA extraction workflow (see Fig. 5) is organized as follows: after obtaining the ESC, the BA can be extracted by combining PUL classifier with only positive samples at same distinguishable orientation; PUL has been proved to be suitable for target extraction tasks with only positive samples [11]. Here, we only randomly select a small number of positive samples with same obvious orientation for PUL, and converts BA extraction problem with only positive samples to learn standard binary classifiers.

The two-step strategy PUL proposed in previous work [11] was applied. First, an improved algorithm yields reliable negative samples from the unlabeled set by cosine similarity with positive samples. Second, a support vector machine iteratively

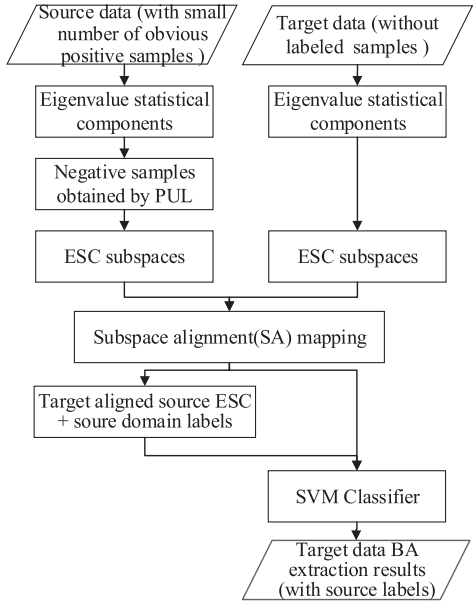

Fig. 6. Proposed workflow of the cross-domain PolSAR BA analysis.

was applied to these negative samples, existing positive samples, and the remaining unlabeled samples. However, there are some differences between the frameworks in Fig. 5 and [11], the applied ESC are different, and the requirements for positive samples are lower, which will be proved by subsequent experiments.

C. ESC-PUL-SA for Cross-Domain PolSAR BA Analysis

In Fig. 3, the traditional $\mathbf{C}3$ and model decomposition features are used to show the domain shift problems in cross-domain PolSAR data. In order to further apply the ESC and positive samples from source domain to achieve cross-domain BA analysis, the workflow in Fig. 6 is presented for the cross-domain BA analysis. It can provide support for BA expansion and change information applications based on multisource and multitemporal PolSAR data, with only a few positive samples available from source data.

Since the unsupervised DA is usually more challenging and practical, combining the description of various DA methods in Section II-C, this article adopts the adapting feature distribution representation approach. More specifically, the classical SA method [33] is selected. The steps in Fig. 6 mainly include: extracting ESC of source and target domain, respectively, the ESC subspaces extraction and SA mapping. The subspaces are obtained by MLE intrinsic dimension estimation [45] and PCA dimensional reduction, and MLE intrinsic dimension $\hat{m}_k$ was estimated as follows:

$$\hat{m}_k = \frac{1}{n}\sum_{i=1}^{n}\hat{m}_k(X_i) \quad (5)$$

$$\hat{m}_k(x) = \left[\frac{1}{k-1}\sum_{j=1}^{k-1}\log\frac{T_k(x)}{T_j(x)}\right]^{-1} \quad (6)$$

TABLE I
DATA DESCRIPTION OF THE EMPLOYED POLSAR DATA

Dataset name	Sensor	Imaging time	Resolution(m)	Size(pixels)	Imaging areas	GT	Purpose
Rs2-Sanf	Radarsat-2	Apr. 2008	8 × 12	1600 × 1200	San Francisco	Yes	BAE[1] & CD[2]
Rs2-Vanc1	Radarsat-2	Apr. 2008	8 × 12	3000 × 1000	Vancouver	Yes	BAE
Rs2-Vanc2	Radarsat-2	Apr. 2008	8 × 12	2600 × 1600	Vancouver	Yes	CD
Rs2-Flev	Radarsat-2	Apr. 2008	8 × 12	1400 × 1200	Flevoland	Yes	CD
Rs2-Wuh1	Radarsat-2	Dec. 2011	8 × 12	5500 × 2400	Wuhan	Yes	BAE
Rs2-Wuh2	Radarsat-2	Dec. 2011	8 × 12	2575 × 2500	Wuhan	Yes	CDE[3]
AS-Sanf	AIRSAR	Jul.1985	8 × 8	900 × 1020	San Francisco	Yes	BAE & CD
US-Sanf	UAVSAR	Nov.2012	5 × 7.2	3300 × 3300	San Diego	No	CD
Gf3-Sanf	Gaofen-3	Sep. 2017	8 × 8	1150 × 1800	San Francisco	Yes	CD
Gf3-Wuh	Gaofen-3	Dec. 2018	8 × 8	3750 × 3600	Wuhan	No	CDE

[1]BAE represents BA extraction experiments from same source.
[2]CD represents cross-domain BA experiments.
[3]CDE represents cross-domain BA expansion experiments.

where n is the number of samples, $T_k(x)$ is the Euclidean distance from a fixed point x to its kth NN in the sample. k is the neighborhood range for MLE intrinsic dimension estimation, whose default value [45] is set to 12.

Then, the original high-dimensional ESC is reduced to ESC subspaces, they are also cross-domain subspaces. ESC subspaces not only retain the most valuable intrinsic features to prevent flooding of effective features, but also cooperate with subspace DA methods and improve operational efficiency. Finally, to achieve cross-domain BA analysis, the SA is further adopted to overcome class distribution shifts between cross-domain data. SA seeks domain invariant feature space by learning a mapping function, which aligns source subspace with the target one [33]. After SA, the aligned source subspaces are close to target subspaces in the Bregman divergence perspective. Also, labeled samples from source domain can be applied to target domain.

IV. EXPERIMENTS AND RESULT ANALYSIS

In this section, the data and settings are first introduced. Then, the ESC-PUL BA extraction and ESC-PUL-SA cross-domain BA analysis performances are also presented. Moreover, the BA expansions of Wuhan optical Valley region, China, from Radarsat-2 and Gaofen-3 data, are further analyzed.

A. Dataset Descriptions and Settings

The effectiveness of the proposed method was tested on six Radarsat-2 spaceborne PolSAR data, two Gaofen-3 spaceborne PolSAR data, an AIRSAR airborne PolSAR data, and an UAV PolSAR data. The basic information selected experimental data are shown in Table I, all the samples from PolSAR data are 50 × 50 pixels patches with 50% or 80% overlapping rate. Figs. 2, 3, and 7 illustrate some composed images by Pauli basis (red for $|hh - vv|^2$, green for $2|hv|^2$, and blue for $|hh + vv|^2$).

These selected datasets from four SAR sensor sources contain typical BA scenes. Datasets including Rs2-Sanf, AS-Sanf, and Gf3-Sanf are from three different sensors; they reflected the same BA scene at different times, and they are often used to analyze BA orientation characteristics in PolSAR. Dataset Rs2-Vanc2 and Rs2-Flev contain more abundant land cover types in different scenes. Dataset Rs2-Wuh1, Rs2-Wuh2, Gf3-Wuh, and US-Sand also contain complex land cover distributions and larger coverage scenarios (Dataset Rs2-Wuh1 covers about 44 × 28.8 km city scenarios), especially they cover BA with almost all orientations and different densities. Higher requirements are put forward for BA extraction algorithm for these datasets. Furthermore, dataset Rs2-Vanc1, Rs2-Wuh1 also contain BA with different densities.

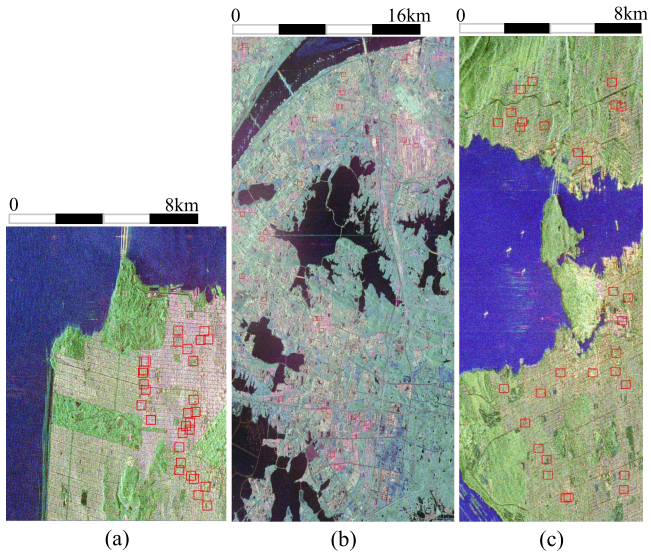

Fig. 7. Pauli images and positive samples of employed data. (a) Rs2-Sanf. (b) Rs2-Vanc. (c) Rs2-Wuh.

The red boxes in Fig. 7 are selected as positive samples. In order to verify the proposed BA extraction can overcome influence of building orientations, we only randomly select the obvious BA samples with typical orientation. The labeled training samples for ESC-PUL BA extractions are less than 0.65% (30/18096, 30/4641, 30/20805). For each cross-domain experimental unit, the positive sample numbers are all set as 60.

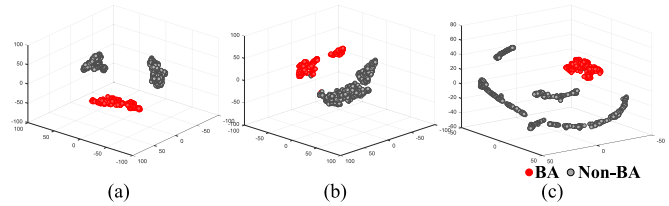

Fig. 8. ESC visualization by t-SNE. (a) Samples from Rs2-Sanf. (b) Samples from AS-Sanf. (c) Samples from Gf3-Sanf.

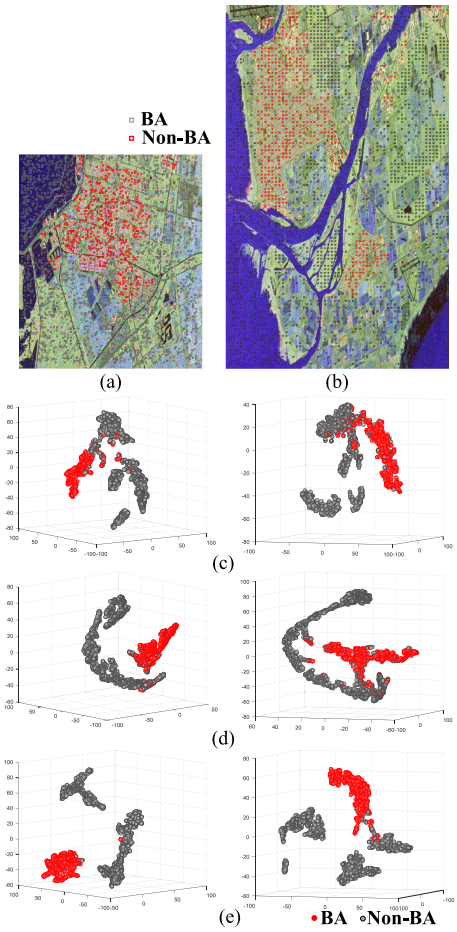

Fig. 9. Features visualization of BA and non-BA samples by t-SNE. (a) Radarsat-2 Flevoland. (b) Radarsat-2 Vancouver. (c) Filtered C3 features of samples. (d) Filtered Yamaguchi decompositions features of samples. (e) ESC visualization of samples in (a) and (b).

Also, the training samples for BA extraction and unsupervised cross-domain BA analysis are all selected randomly.

B. ESC-PUL BA Extraction Performances

To illustrate effectiveness of the proposed ESC, Fig. 8 shows the ESC of BA and non-BA samples in Fig. 3 by t-SNE. In Fig. 3(d) and (e), there are serious intraclass differences between the traditional C3 and decomposition component features, while the intraclass clusterings of ESC in Fig. 8 are more satisfactory. In addition, Fig. 9 further verifies advantages of the proposed ESC features compared with traditional features by Rs2-Vanc2 and Rs2-Flev data.

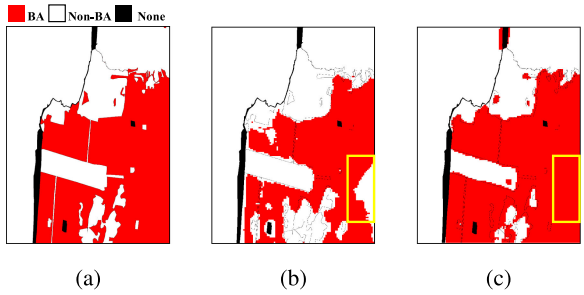

Fig. 10. Ground truth of Rs2-Sanf and BA extraction results. (a) Ground truth. (b) SMSF-PUL. (c) Proposed method.

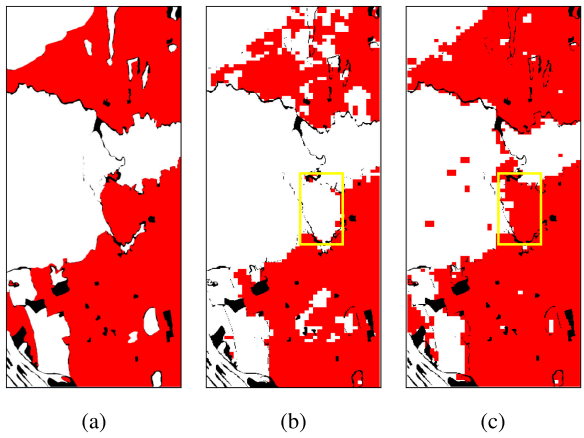

Fig. 11. Ground truth of Rs2-Vanc and BA extraction results. (a) Ground truth. (b) SMSF-PUL. (c) Proposed method.

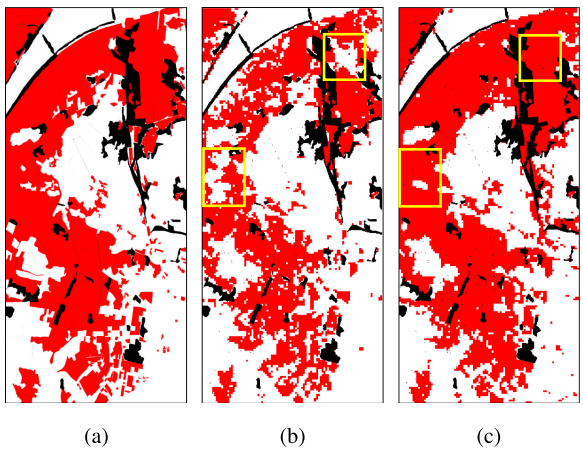

Fig. 12. Ground truth of Rs2-Wuh and BA extraction results. (a) Ground truth. (b) SMSF-PUL. (c) Proposed method.

Figs. 10(a)–12(a) showed the ground truths of datasets in Fig. 7. The BA extraction results by our previous works [11]—deoriented Yamaguchi decomposition feature and PUL (SMSF-PUL) are the comparative experiments, as illustrated in Figs. 10(b)–12(b). Also, the results of the proposed method have been shown in Figs. 10(c)–12(c). As can be seen from abovementioned three experimental results, under the condition

TABLE II
QUANTITATIVELY EVALUATION OF BA EXTRACTION

Data	Method	BA-acc.(%)	OA.(%)	F
Rs2-Sanf	C3D-PUL	79.40	89.66	0.8634
	SMSF-PUL	78.46	89.54	0.8710
	Azmedroub(2016)	82.26	89.89	0.8730
	Susaki(2016)	88.43	91.98	0.8958
	Proposed	**98.84**	**94.89**	**0.9455**
Rs2-Vanc	C3D-PUL	69.34	79.18	0.8041
	SMSF-PUL	77.81	86.77	0.8658
	Azmedroub(2016)	27.34	54.60	0.4075
	Susaki(2016)	60.27	74.62	0.7371
	Proposed	**97.30**	**92.89**	**0.9376**
Rs2-Wuh	C3D-PUL	66.25	74.49	0.7640
	SMSF-PUL	74.38	84.40	0.8166
	Azmedroub(2016)	60.98	76.52	0.7281
	Susaki(2016)	56.56	69.77	0.6781
	Proposed	**92.64**	**87.82**	**0.8766**
Rs2-Flev	C3D-PUL	98.42	87.75	0.6443
	SMSF-PUL	75.81	92.80	0.8371
	Azmedroub(2016)	88.56	81.18	0.5655
	Susaki(2016)	99.08	84.91	0.5455
	Proposed	**93.33**	**91.62**	**0.8447**
As-Sanf	C3D-PUL	95.46	88.20	0.8511
	SMSF-PUL	73.03	86.52	0.8348
	Azmedroub(2016)	84.84	86.50	0.8352
	Susaki(2016)	95.44	75.44	0.6426
	Proposed	**94.53**	**92.24**	**0.9191**

BA-acc. represents accuracy of BA extraction, OA. means the overall accuracy of BA and non-BA, F value measures the performance of a system on a particular class (BA in this case). $F = 2PR/(P+R)$, where P is the precision and R is the recall.
The bold values represent the higher accuracies than the comparison methods.

that the positive samples only contains single orientation, the model decomposition-based features are difficult to overcome the influence of multiple orientations, which may result in incomplete extraction or misclassification of BA [as shown in the yellow boxes in Figs. 10(b)–12(b)]. Under the same conditions, the proposed method performs more accurate results, despite there are only a small number of positive samples with single orientation available. The quantitatively evaluations of BA extraction results are listed in Table II.

To further verify the effectiveness and reliability of the proposed method, experiments on data with more complex backgrounds, airborne PolSAR data are conducted. Three groups of comparative experiments are added and analyzed. First, two state-of-the-art methods, including the BA extraction method of Azmedroub *et al.* [46] [i.e., Azmedroub's (2016)] and the method of Susaki and Kishimoto [47] [i.e., Susaki's (2016)] are applied. They have been cited and compared in many recent PolSAR BA extraction papers [47], [48]. Method Azmedroub's (2016) does not need labeled samples, whereas method Susaki's (2016) needs labeled samples with BA and forests for training. In detail, method Azmedroub's (2016) extracts BA based on pixels, it uses surface scattering power (Ps), the double-bounce scattering power (Pd), and volume scattering power (Pv) from Yamaguchi decomposition after filtering and POA compensation. Method Susaki's (2016) is based on regional features, including total power, Pv, and polarimetric coherence.

Second, in order to further verify the advantages of polarimetric eigenvalues for PolSAR BA extraction compared with other features, and to illustrate the generalization of this statistical feature model, we use the diagonal elements of C3 matrix to carry out the Wishart statistical analysis, and then extract BA with PUL under the same conditions. This group of experiments is named C3D-PUL as another comparative experiment. The improved experimental validations are shown in Table II and Fig. 13. Not all of the compared result maps are displayed here, for the sake of space.

Among these data, Rs2-Sanf, Rs2-Flev, and AS-Sanf data are commonly used datasets. The results of comparison methods [46], [47] on these typical datasets are comparable with the results reported in the corresponding papers [47], [48]. This shows that the comparisons are objective. However, due to the complex BA orientations and distributions, these two methods are not work well on Rs2-Van and Rs2-Wuh. From Table II, the results of Susaki's (2016) performances better than that of Azmedroub's (2016), since Susaki's (2016) applied two kinds of labeled samples. In addition, C3D-PUL has similar effect with SMSF-PUL. The proposed BA extraction method is feasible for typical PolSAR images BA extraction tasks with accuracies of 92%–98%, 8%–20% higher than SMSF-PUL, under the condition that only the small number of positive labeled samples is available.

The comparison method Susaki's (2016), C3D-PUL, SMSF-PUL, and the proposed method apply regional features, which show that the performances of regional features are better than that of pixel level features [Azmedroub's (2016)] for applied PolSAR data. In addition, methods Susaki's (2016), C3D-PUL, and SMSF-PUL involve the original polarimetric features, polarimetric decompositions, and polarimetric coherence, which are not roll-invariant. Based on the abovementioned comparison experiments and analysis, the main factor that improves the proposed BA analysis performance lies in comprehensive use of roll-invariant features and regional statistical features. In the subsequent cross-domain experiments, ESC-PUL will be used as a comparative experiment, which can further prove its effectiveness in more datasets.

C. ESC-PUL-SA Cross-Domain BA Analysis Performances

Since the applied datasets have different characteristics, to verify the effectiveness of proposed cross-domain BA analysis strategy, 14 cross-domain experimental units are conducted, including the different scenes data from same sensors, the same/similar scenes data from different sensors, and the different scenes data from different sensors. The details of cross-domain experimental units are presented in Table III. Moreover, Fig. 14 shows the cross-domain process in Fig. 6 by t-SNE view and the samples from RS2-Sanf and GF3-Sanf. After ESC extraction and SA, the BA and non-BA feature distributions in source domain are basically the same as that in target domain, achieving the effect of reducing domain shifts and reusing labeled samples.

The positive training samples from source domain are selected randomly. For each cross-domain experimental unit, the number of positive samples is 60, the random selected labeled training samples are less than 1.30%, and the unlabeled sets are also randomly selected. The settings of comparative experiments are also presented as following,

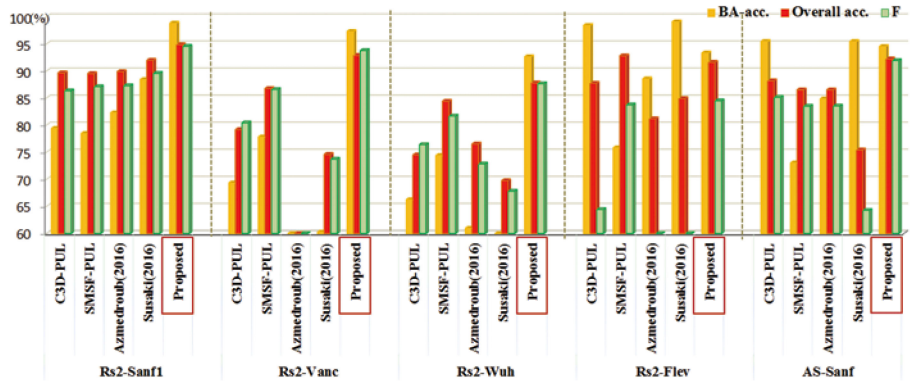

Fig. 13. Quantitatively evaluates BA extraction accuracy and comparative evaluation.

TABLE III
CROSS-DOMAIN RESULTS OF PROPOSED METHOD AND COMPARISONS

Units	ESC-PUL-D	ESC-PUL-GFK	**Proposed**	Target-PUL
Rs2-Sanf⇒ Gf3-Sanf	53.84	57.49	**91.31**	92.07
Gf3-Sanf⇒ Rs2-Sanf	74.46	83.00	**94.48**	98.84
Rs2-Sanf ⇒ AS-Sanf	70.09	51.90	**92.99**	94.53
AS-Sanf ⇒ Rs2-Sanf	78.52	83.09	**94.44**	98.84
Gf3-Sanf ⇒ AS-Sanf	84.36	42.42	**92.02**	94.53
AS-Sanf ⇒ Gf3-Sanf	85.67	54.37	**91.67**	92.07
Rs2-Sanf ⇒ Rs2-Wuh1	77.76	74.18	**89.64**	92.64
Rs2-Wuh1 ⇒ Rs2-Sanf	87.12	48.39	**93.55**	98.84
US-Sand ⇒ Rs2-Sanf	77.70	87.13	**92.90**	93.33
US-Sand ⇒ AS-Sanf	74.87	82.56	**91.62**	94.53
Rs2-Flev ⇒ Rs2-Vanc2	81.56	77.45	**95.53**	95.16
Rs2-Vanc2 ⇒ Rs2-Flev	85.99	70.07	**93.40**	93.33
Rs2-Sanf⇒ Rs2-Flev	89.87	76.20	**90.62**	93.33
Rs2-Flev ⇒ Rs2-Sanf	74.98	55.00	**93.64**	98.84

[1]"⇒" indicates samples from source domain A used in target domain B.
The bold values represent the higher accuracies than the comparison methods.

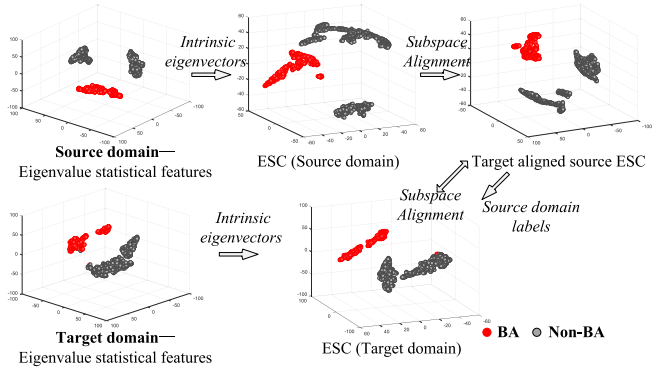

Fig. 14. SA of ESC features in source and target domains by t-SNE visualization.

1) ESC-PUL-D: By using ESC and PUL to learn negative samples in source domain, then, the learned samples and labeled samples from source domain are directly applied for target domain, without applying SA. The comparison between this method and the proposed method can prove that SA mapping is necessary and reasonable for the proposed cross-domain framework.

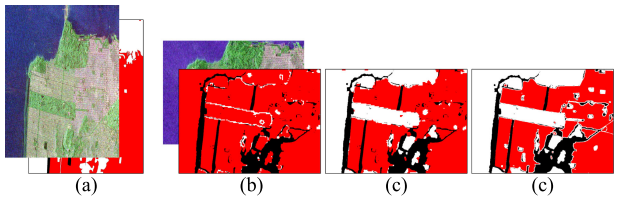

Fig. 15. Cross-domain results of Gf3-Sanf data, with Rs2-sanf data as source domain. (a) Source data. Results of (b) ESC-PUL-GFK, (c) proposed ESC-PUL-SA, and (d) GT.

2) ESC-PUL-GFK: Another classic unsupervised DA method, geodesic flow kernel (GFK) [49], was applied as another comparative method. The applied features are ESCs, and the training samples settings are same as that in the proposed method experiments.
3) Target-PUL: ESC-PUL BA extraction by target positive samples is conducted. These comparison experiments can verify the ESC-PUL-SA cross-domain BA analysis in Fig. 6, which are comparable with the effects of target ESC-PUL. ESC-PUL-SA can reduce the differences caused by sensors and imaging scenes. Also, this setting can further verify the effectiveness of the proposed ESC-PUL BA extraction. The number of positive samples is 60 in this group of experiments.

The cross-domain results of 14 units are shown in Table III and with results of comparative experiments. As can be seen, the results of ESC-PUL-SA are better than ESC-PUL-D and ESC-PUL-GFK in whole, and it can almost achieve similar effect of Target-PUL. Results of Rs2-sanf data as the source domain, and Gf3-Sanf and AS-Sanf dataset as target domain are illustrated in Figs. 15 and 16, respectively (to save space, only the results of ESC-PUL-GFK, proposed method, and GT are presented). Fig. 17 shows cross-domain results of Rs2-Van2 and Rs2-Flev datasets. The cross-domain BA extraction accuracies of 14 units ranged from 89.64% to 95.53%. The abovementioned cross-domain experiment results prove that the proposed ESC-PUL-SA is a robust and promising cross-domain BA analysis method for PolSAR imageries, and it can obtain accurate BA expansion and change information from multidomain PolSAR data with only few BA samples from one source data.

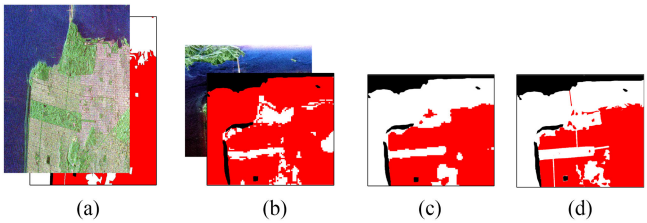

Fig. 16. Cross-domain results of AS-Sanf data, with Rs2-sanf data as source domain. (a) Source data. Results of (b) ESC-PUL-GFK, (c) proposed ESC-PUL-SA, and (d) GT.

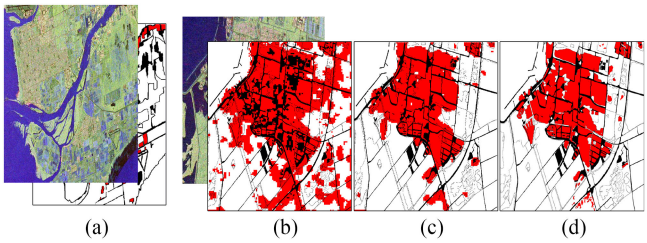

Fig. 17. Cross-domain results of Rs2-Flev data, with Rs2-Van2 data as source domain. (a) Source data. Results of (b) ESC-PUL-GFK, (c) proposed ESC-PUL-SA, and (d) GT.

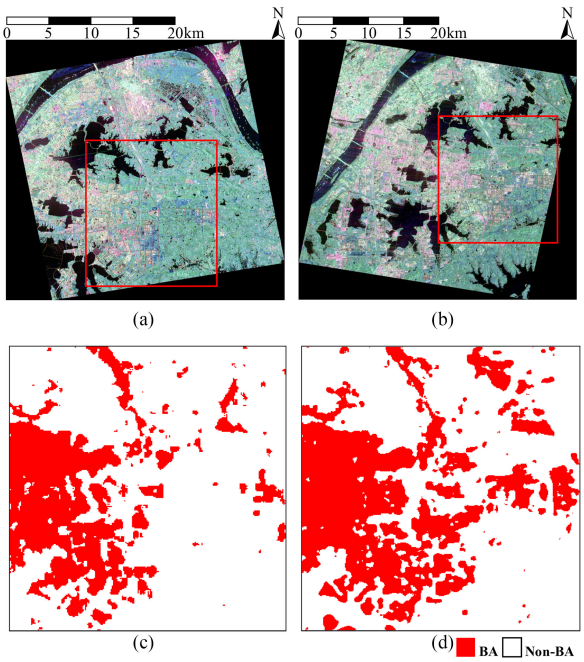

Fig. 18. Cross-domain BA expansion analysis in Wuhan Optical Valley. (a) Radarsat-2 Wuhan data. (b) Gaofen-3 Wuhan data. (c) Radarsat-2 Wuhan BA extraction by ESC-PUL. (d) Cross-domain BA analysis results by ESC-PUL-SA in Gaofen-3 Wuhan data with samples from Radarsat-2 Wuhan data.

D. Cross-Domain BA Expansion of Wuhan Optical Valley Region

To further verify the proposed cross-domain method for obtaining BA expansion information, the cross-domain BA analysis in Wuhan Optical Valley area from Radarsat-2 and Gaofen-3 PolSAR data is conducted. Specifically, the PolSAR data that contain the same areas obtained by Radarsat-2 in 2011 and Gaofen-3 in 2018 were selected, only a small number of positive samples from source domain Radarsat-2 data are available. Fig. 18 shows the data and cross-domain results.

In this cross-domain group, only Rs2-Wuh2 data with BA labels, the BA extraction accuracy in Fig. 18(c) is 94.60%, the overall accuracy is 91.39%, and the F value is 0.8024. Since Gf3-Wuh data lack GT, and this cross-domain BA analysis is conducted based on labeled samples from Rs2-Wuh2. It is obvious that the BA in east and south of Wuhan Optical Valley has expanded a lot after years of development. This obtained BA expansion information is consistent with the development trends of Wuhan city.

V. Conclusion

In this article, the problems of PolSAR imagery BA extraction affected by building orientation effect and depended on abundant labeled samples were first studied. Based on roll-invariant eigenvalue statistical information and PUL, the proposed BA extraction method was conducted on Radarsat-2, Gaofen-3, and AIRSAR PolSAR images. Experimental results showed that the accuracy can reach 92%–98% with only positive training samples less than 0.65%, 8%–20% higher than the traditional model decomposition-based PUL method at same settings. The proposed method can overcome BAs misdetection caused by large orientation angles and reduce requirements for many labeled samples.

Furthermore, the eigenvalue statistical information and PUL were further extended to the unsupervised cross-domain BA analysis, with only positive samples from the source domain available. The cross-domain BA extraction accuracies of 14 units are ranged from 89.64% to 95.53%. It not only verifies the effectiveness of proposed features and PUL for the BA analysis, but also provides a strong support for BA expansion and change analysis from multisource and multi-temporal PolSAR data, with a few positive samples from source data. Follow-up study is to focus on building density, urban functional area classification, and more specific building change information extraction from PolSAR data.

References

[1] L. Wang *et al.*, "Mapping population density in China between 1990 and 2010 using remote sensing," *Remote Sens. Environ.*, vol. 210, pp. 269–281, Jun. 2018.

[2] G. Iannelli and P. Gamba, "Urban extent extraction combining sentinel data in the optical and microwave range," *IEEE J. Sel. Topics Appl. Earth Observ. Remote Sens.*, vol. 12, no. 7, pp. 2209–2216, Jul. 2019.

[3] D. Verma, A. Jana, and K. Ramamritham, "Transfer learning approach to map urban slums using high and medium resolution satellite imagery," *Habitat Int.*, vol. 88, Jun. 2019, Art. no. 101981.

[4] S. Chen, X. Wang, and S. Xiao, "Urban damage level mapping based on co-polarization coherence pattern using multitemporal polarimetric SAR data," *IEEE J. Sel. Topics Appl. Earth Observ. Remote Sens.*, vol. 11, no. 8, pp. 2657–2667, Aug. 2018.

[5] Y. Ji, J. Sumantyo, M. Chua, and M. Waqar, "Earthquake/tsunami damage level mapping of urban areas using full polarimetric SAR data," *IEEE J. Sel. Topics Appl. Earth Observ. Remote Sens.*, vol. 11, no. 7, pp. 2296–2309, Jul. 2018.

[6] A. Salentinig and P. Gamba, "Combining SAR-based and multispectral-based extractions to map urban areas at multiple spatial resolutions," *IEEE Geosci. Remote Sens. Mag.*, vol. 3, no. 3, pp. 100–112, Sep. 2015.

[7] S. De, L. Bruzzone, A. Bhattacharya, F. Bovolo, and S. Chaudhuri, "A novel technique based on deep learning and a synthetic target database for classification of urban areas in PolSAR data," *IEEE J. Sel. Topics Appl. Earth Observ. Remote Sens.*, vol. 11, no. 1, pp. 154–170, Jan. 2018.
[8] X. Sun, H. Song, R. Wang, and N. Li, "High-resolution polarimetric SAR image decomposition of urban areas based on a POA correction method," *Remote Sens. Lett.*, vol. 9, no. 4, pp. 363–372, Jan. 2018.
[9] S. Quan, B. Xiong, D. Xiang, C. Hu, and G. Kuang, "Scattering characterization of obliquely oriented buildings from PolSAR data using eigenvalue-related model," *Remote Sens.*, vol. 11, no. 5, Mar. 2019, Art. no. 581.
[10] J. Chen, H. Zhang, C. Wang, and J. Jia, "Roll-invariant target parameter extraction from POLSAR data," *IEEE J. Sel. Topics Appl. Earth Observ. Remote Sens.*, vol. 12, no. 11, pp. 4502–4516, Nov. 2019.
[11] W. Yang, X. Yin, H. Song, Y. Liu, and X. Xu, "Extraction of built-up areas from fully polarimetric SAR imagery via PU learning," *IEEE J. Sel. Topics Appl. Earth Observ. Remote Sens.*, vol. 7, no. 4, pp. 1207–1216, Dec. 2013.
[12] Y. Tan, S. Xiong, and Y. Li, "Automatic extraction of built-up areas from panchromatic and multispectral remote sensing images using double-stream deep convolutional neural networks," *IEEE J. Sel. Topics Appl. Earth Observ. Remote Sens.*, vol. 11, no. 11, pp. 3988–4004, Oct. 2018.
[13] S. Chen, X. Wang, S. Xiao, and M. Sato, *Target Scattering Mechanism in Polarimetric Synthetic Aperture Radar: Interpretation and Application*. Singapore: Springer, 2018.
[14] H. Fan, S. Quan, D. Dai, and S. Xiao, "Refined model-based and feature-driven extraction of buildings from PolSAR images," *Remote Sens.*, vol. 11, no. 11, Jun. 2019, Art. no. 1379.
[15] S. Quan, B. Xiong, D. Xiang, and G. Kuang, "Derivation of the orientation parameters in built-up areas: With application to model-based decomposition," *IEEE Trans. Geosci. Remote Sens.*, vol. 56, no. 8, pp. 4714–4730, Aug. 2018.
[16] S. Chen, X. Wang, S. Xiao, and M. Sato, "General polarimetric model-based decomposition for coherency matrix," *IEEE Trans. Geosci. Remote Sens.*, vol. 52, no. 3, pp. 1843–1855, Mar. 2014.
[17] S. Quan, B. Xiong, D. Xiang, L. Zhao, S. Zhang, and G. Kuang, "Eigenvalue-based urban area extraction using polarimetric SAR data," *IEEE J. Sel. Topics Appl. Earth Observ. Remote Sens.*, vol. 11, no. 2, pp. 458–471, Feb. 2018.
[18] P. Du, A. Samat, B. Waske, S. Liu, and Z. Li, "Random forest and rotation forest for fully polarized SAR image classification using polarimetric and spatial features," *ISPRS J. Photogrammetry Remote Sens.*, vol. 105, pp. 38–53, Jul. 2015.
[19] S. Gou, X. Qiao, X. Zhang, W. Wang, and F. Du, "Eigenvalue analysis-based approach for POL-SAR image classification," *IEEE Trans. Geosci. Remote Sens.*, vol. 52, no. 2, pp. 805–818, Feb. 2014.
[20] S. Zhang, S. Wang, B. Chen, and S. Mao, "Classification method for fully PolSAR data based on three novel parameters," *IEEE Geosci. Remote Sens. Lett.*, vol. 11, no. 1, pp. 39–43, Jan. 2014.
[21] R. Sato, Y. Ikarashi, M. Masaka, Y. Yamaguchi, and H. Yamada, "Polarimetric scattering analysis for detecting largely-oriented man-made objects based on eigenvalues/eigenvectors analysis to the rotated coherency matrix," in *Proc. IEEE Int. Geosci. Remote Sens. Symp.*, Jul. 2015, pp. 3810–3813.
[22] J. Chen, H. Zhang, C. Wang, and J. Jia, "Roll-invariant target parameter extraction from POLSAR data," *IEEE J. Sel. Topics Appl. Earth Observ. Remote Sens.*, vol. 12, no. 11, pp. 4502–4516, Nov. 2019.
[23] X. Leng, K. Ji, S. Zhou, X. Xing, and H. Zou, "Discriminating ships from radio frequency interference based on non-circularity and non-Gaussianity in Sentinel-1 SAR imagery," *IEEE Trans. Geosci. Remote Sens.*, vol. 57, no. 1, pp. 352–363, Jan. 2019.
[24] R. Gui, X. Xu, L. Wang, R. Yang, and F. Pu, "A generalized zero-shot learning framework for PolSAR land cover classification," *Remote Sens.*, vol. 10, no. 8, Aug. 2018, Art. no. 1307.
[25] M. Babaee, S. Tsoukalas, G. Rigoll, and M. Datcu, "Visualization-based active learning for the annotation of SAR images," *IEEE J. Sel. Topics Appl. Earth Observ. Remote Sens.*, vol. 8, no. 10, 4687–4698, Oct. 2015.
[26] L. Du, H. Dai, Y. Wang, W. Xie, and Z. Wang, "Target discrimination based on weakly supervised learning for high-resolution SAR images in complex scenes," *IEEE Trans. Geosci. Remote Sens.*, vol. 58, no. 1, 461–472, Jan. 2020.
[27] H. Dong H, X. Xu, R. Yang, and F. Pu, "Component ratio-based distances for cross-source PolSAR image classification," *IEEE Geosci. Remote Sens. Lett.*, vol. 17, no. 5, pp. 824–828, May 2020.
[28] X. Qin, J. Yang, P. Li, W. Sun, and W. Liu, "A novel relational-based transductive transfer learning method for PolSAR images via TimeSeries clustering," *Remote Sens.*, vol. 11, no. 11, Jun. 2019, Art. no. 1358.
[29] D. Tuia, C. Persello, and L. Bruzzone, "Domain adaptation for the classification of remote sensing data: An overview of recent advances," *IEEE Geosci. Remote Sens. Mag.*, vol. 4, no. 2, pp. 41–57, Jun. 2016.
[30] F. Denis, "PAC learning from positive statistical queries," in *Proc. Int. Conf. Algorithmic Learn. Theory*, 1998, pp. 112–126.
[31] E. Sansone, F. De Natale, and Z. Zhou, "Efficient training for positive unlabeled learning," *IEEE Trans. Pattern Anal. Mach. Intell.*, vol. 41, no. 11, pp. 2584–2598, Nov. 2019.
[32] J. Zhang, Z. Wang, J. Meng, Y. Tan, and J. Yuan, "Boosting positive and unlabeled learning for anomaly detection with multi-features," *IEEE Trans. Multimedia*, vol. 21, no. 5, pp. 1332–1344, May 2019.
[33] B. Fernando, A. Habrard, M. Sebban, and T. Tuytelaars, "Unsupervised-visual domain adaptation using subspace alignment," in *Proc. IEEE Int. Conf. Comput. Vis.*, Dec. 2013, pp. 2960–2967.
[34] W. Kouw and M. Loog, "A review of domain adaptation without target labels," *IEEE Trans. Pattern Anal. Mach. Intell.*, to be published, doi: 10.1109/TPAMI.2019.2945942.
[35] R. Gui, X. Xu, D. Zhang, L. Wang, R. Yang, and P. Fu, "Built-up areas extraction from PolSAR imagery via eigenvalue statistical information and pu-learning," in *Proc. IEEE Int. Geosci. Remote Sens. Symp.*, 2019, pp. 1196–1199.
[36] H. Kimura, "Radar polarization orientation shifts in built-up areas," *IEEE Geosci. Remote Sens. Lett.*, vol. 5, no. 2, pp. 217–221, Apr. 2008.
[37] J. S. Lee and E. Pottier, *Polarimetric Radar Imaging: Basics to Applications*, 2nd ed. Boca Raton, FL, USA: CRC Press, 2016.
[38] C. Elkan and K. Noto, "Learning classifiers from only positive and unlabeled data," in *Proc. ACM SIGKDD Int. Conf. Knowl. Discovery Data Mining*, 2008, pp. 213–220.
[39] J. Zhou, S. Pan, Q. Mao, and I. Tsang, "Multi-view positive and unlabeled learning," *J. Mach. Learn. Res.*, vol. 25, pp. 555–570, Jan. 2012.
[40] R. Liu, W. Li, X. Liu, X. Lu, T. Li, and Q. Guo, "An ensemble of classifiers based on positive and unlabeled data in one-class remote sensing classification," *IEEE J. Sel. Topics Appl. Earth Observ. Remote Sens.*, vol. 11, no. 2, pp. 572–584, Feb. 2018.
[41] J. Zhang, Z. Wang, J. Meng, Y. Tan, and J. Yuan, "Boosting positive and unlabeled learning for anomaly detection with multi-features," *IEEE Trans. Multimedia*, vol. 21, no. 5, pp. 1332–1344, May 2018.
[42] F. Ye, W. Luo, M. Dong, H. He, and W. Min, "SAR Image retrieval based on unsupervised domain adaptation and clustering," *IEEE Geosci. Remote Sens. Lett.*, vol. 16, no. 9. pp. 1482–1486, Mar. 2019.
[43] D. Malmgren-Hansen, A. Kusk, J. Dall, A.-A. Nielsen, R. Engholm, and H. Skriver, "Improving SAR automatic target recognition models with transfer learning from simulated data," *IEEE Geosci. Remote Sens. Lett.*, vol. 14, no. 9, pp. 1484–1488, Sep. 2017.
[44] L. V. Der Maaten and G. E. Hinton, "Visualizing data using t-SNE," *J. Mach. Learn. Res.*, vol. 9, pp. 2579–2605, 2008.
[45] E. Levina and P.-J. Bickel, "Maximum likelihood estimation of intrinsic dimension," in *Proc. 17th Int. Conf. Neural Inf. Process. Syst.*, Jan. 2004, pp. 777–784.
[46] B. Azmedroub, M. Ouarzeddine, and B. Souissi, "Extraction of urban areas from polarimetric SAR imagery," *IEEE J. Sel. Topics Appl. Earth Observ. Remote Sens.*, vol. 9, no. 6, pp. 2583–2591, Apr. 2016.
[47] J. Susaki and M. Kishimoto, "Urban area extraction using X-band fully polarimetric SAR imagery," *IEEE J. Sel. Topics Appl. Earth Observ. Remote Sens.*, vol. 9, no. 6, pp. 2592–2601, Apr. 2016.
[48] S. Quan, B. Xiong, D. Xiang, L. Zhao, S. Zhang, and G. Kuang, "Eigenvalue-based urban area extraction using polarimetric SAR data," *IEEE J. Sel. Topics Appl. Earth Observ. Remote Sens.*, vol. 11, no. 2, pp. 458–471, Feb. 2018.
[49] B. Gong, Y. Shi, F. Sha, and K. Grauman, "Geodesic flow kernel for unsupervised domain adaptation," in *Proc. IEEE Conf. Comput. Vision Pattern Recognit.*, 2012, pp. 2066–2073.

Rong Gui (Graduate Student Member, IEEE) received the M.E. degree, in 2016 from Wuhan University, Wuhan, China, where she is currently working toward the Ph.D. degree in signal and information processing.

Her research interests include SAR imagery processing, 3-D laser measurement technology, and pattern recognition.

Xin Xu received the B.S. degree in electronic engineering, the M.S. degree in signal and information processing, and the Ph.D. degree in photogrammetry and remote sensing from Wuhan University, Wuhan, China, in 1989, 1996, and 2003, respectively.

He is currently a Professor with the School of Electronic Information, Wuhan University. His research interests include image understanding and statistical signal processing with applications to remote sensing.

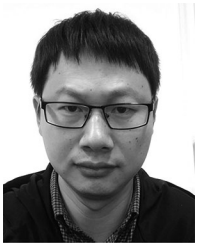

Lei Wang (Member, IEEE) received the B.S. degree in circuit and system and the M.S. degree in communication engineering, in 2009 and 2011, respectively, from Wuhan University, Wuhan, China, where he is currently working toward the Ph.D. degree with the School of Electronic Information.

His research interests include deep learning and polarimetric SAR image processing.

Rui Yang (Graduate Student Member, IEEE) received the B.Eng. degree in electronic engineering, in 2017 from Wuhan University, Wuhan, China, where he is currently working toward the Ph.D. degree in signal and information processing.

His research interests include machine learning and computer vision, especially applications on remote sensing imagery processing.

Fangling Pu (Member, IEEE) received the Ph.D. degree in photogrammetry and remote sensing from Wuhan University, Wuhan, China, in 2005.

She was a Research Assistant with the Institute for Theoretical Information Technology, RWTH Aachen University, in 2007. Since 2000, she has been an Associate Professor with the School of Electronic Information, Wuhan University. Her research interests include system and networking, signal and information processing, and data mining.